coatings

MDPI

Article

Atomic Layer Deposition of Y_2O_3 Thin Films Using $Y(MeCp)_2(iPr\text{-}nPrAMD)$ Precursor and H_2O, and Their Erosion Resistance in CF_4-Based Plasma

Seong Lee [1], Hyunchang Kim [2] and Sehun Kwon [1,*]

[1] School of Materials Science and Engineering, Pusan National University, Busan 46241, Republic of Korea; castlecastle@pusan.ac.kr
[2] iChems Co., Ltd., 73, Banjeong-ro 204beon-gil, Hwaseong-si 18374, Republic of Korea; hckim@ichems.co.kr
* Correspondence: sehun@pusan.ac.kr

Abstract: Atomic layer deposition (ALD) of Y_2O_3 thin films was investigated using $Y(MeCp)_2(iPr\text{-}nPrAMD)$ precursor and H_2O reactant. The self-limiting reaction mechanism of ALD-Y_2O_3 thin films was confirmed at a growth temperature of 260 °C. And, the saturated growth rate was confirmed to be ~0.11 nm/cycle. Also, it was demonstrated that a wide ALD temperature window from 150 °C to 290 °C maintains a consistent growth rate. ALD-Y_2O_3 thin films were found to have a typical cubic polycrystalline structure, independent of growth temperature, which can be attributed to their stoichiometric composition of Y_2O_3, negligible carbon impurity, and high film density, analogous to the Y_2O_3 bulk. Even at a low growth temperature of 150 °C, ALD-Y_2O_3 exhibited a markedly lower plasma etching rate (~0.77 nm/min) than that (~4.6 nm/min) of ALD-Al_2O_3 when using RIE at a plasma power of 400 W with a mixed gas of $Ar/CF_4/O_2$. Furthermore, the growth temperature of Y_2O_3 thin films had minimal impact on the etching rate.

Keywords: Y_2O_3 thin film; atomic layer deposition; CF_4 plasma; protective coating

Academic Editor: Paolo Mele

Received: 12 December 2024
Revised: 24 December 2024
Accepted: 26 December 2024
Published: 30 December 2024

Citation: Lee, S.; Kim, H.; Kwon, S. Atomic Layer Deposition of Y_2O_3 Thin Films Using $Y(MeCp)_2(iPr\text{-}nPrAMD)$ Precursor and H_2O, and Their Erosion Resistance in CF_4-Based Plasma. *Coatings* **2025**, *15*, 22. https://doi.org/10.3390/coatings15010022

1. Introduction

In the semiconductor industry, semiconductor devices with smaller feature sizes are more sensitive to particle and metal contamination, making this an important area of focus. For example, three-dimensional vertical NAND(3D V NAND) technology is being used to stack circuits in multiple layers by reducing the integrated circuit line width directly on the wafer. Therefore, the dry etching process uses fluorocarbon-based high-density plasma performed repeatedly in the chamber and at the same time, ceramic equipment components are exposed to plasma atmosphere [1]. Furthermore, fluorocarbon plasma bombards and erodes the inner-wall materials of the equipment parts [2–6]. In particular, the showerhead facing the wafer can undergo significant etching in a harsh, high-density plasma flux. This erosion of equipment components and the generation of contaminant particles causes serious problems, such as reducing the yield in mass production [6]. Thus, the development of advanced protective coating materials, along with proper deposition techniques, has recently become the focus of intensive efforts to minimize equipment component erosion and contaminant particle generation. A core requirement for coatings on equipment components is that the coating itself should not release particles and should not contain metal contaminants. Therefore, it must exhibit high resistance to corrosion and erosion under various chemical and plasma conditions. Corrosion can be mitigated through the use of ceramic coatings, which offer exceptional resistance to fluorine plasma.

To protect semiconductor components from plasma erosion and the formation of particle contaminants, oxide ceramics such as Al_2O_3 and SiO_2 are commonly used as plasma-resistant materials. However, the performance of Al_2O_3 and SiO_2 coatings has become increasingly problematic due to the higher power levels in fluorine-based plasma equipment. Additionally, these materials are shown to be vulnerable to the fluorine-based plasma etching process when subjected to repeated cycles in a chamber. To address this issue, yttrium oxide (Y_2O_3) has increasingly been proposed as a widely used protective coating material because of its significantly lower etching rate and low chemical reactivity [1,7–10]. Y_2O_3 has many favorable properties making it highly attractive for various industrial applications. These properties include a wide energy band gap (5.5 eV~5.8 eV) and band offset (2.3 eV), a relatively high dielectric constant (14~18), a high refractive index (1.9), a high melting point (2430 °C) that ensures excellent thermal stability, and good thermal conductivity (κ = 0.33 W cm^{-1} K^{-1}) [11,12]. Notably, Y_2O_3 possesses impressive wear resistance, and high mechanical and dielectric strength, as well as superior corrosion and chemical resistance, making it an ideal choice for a protective coating in fluorine-based plasma equipment components [11–15].

Up to now, Y_2O_3 protective coating has been extensively studied using various deposition techniques, such as atmosphere plasma spray (APS) [16], vacuum plasma spray (VPS) [17], physical vapor deposition (PVD) [18], and chemical vapor deposition (CVD) [19]. However, defects such as pore generation, impurities, and poor conformality still need to be addressed in order to improve their protective performance and reduce the coating thickness. In this regard, the atomic layer deposition (ALD) technique has recently attracted attention as a feasible method for forming Y_2O_3 protective coatings. In this process, precursor molecules in the gaseous state are introduced into a chamber, where they react with the substrate surface to grow thin films in a layer-by-layer fashion. The key advantage of ALD lies in its atomic-scale deposition and inherently self-limiting growth mechanism, offering several benefits, including precise atomic-scale thickness control, completely conformal and pinhole-free coatings, and excellent step coverage in highly complex structures [20–22]. Moreover, a recent development of batch-type ALD equipment [23] is accelerating the application of the ALD protective layer in large-scale components. ALD-Y_2O_3 has been demonstrated by using various precursors including $Y(MeCp)_3$ [24], $Y(EtCp)_3$ [25], $Y(iPrCp)_3$ [26], $Y(thd)_3$ [27–30], and $Y(EtCp)_2(iPr_2\text{-amd})$ [31], and oxidants such as H_2O and O_3. However, most ALD-Y_2O_3 studies have primarily focused on high-k dielectric applications, with only a few studies [31] reporting its anti-corrosion properties against fluorine-based plasma. Additionally, the relatively narrow ALD temperature window of some precursors [24–26] needs further improvement, as it may restrict its potential for a broader range of industrial applications. For example, the ALD temperature window for $Y(MeCp)_3$ was 250–300 °C [24]. $Y(EtCp)_3$ and $Y(iPrCp)_3$ also exhibited narrow ALD temperature windows (250–280 °C for $Y(EtCp)_3$ and 245–300 °C for $Y(iPrCp)_3$) [25,26]. For the $Y(EtCp)_2(iPr_2\text{-amd})$ precursor, the ALD temperature window was 300–450 °C, which may restrict low-temperature applications. On the other hand, $Y(thd)_3$ showed a relatively wide ALD temperature window from 250 to 375 °C. However, high carbon and hydrogen impurities were also reported for $Y(thd)_3$ [27–30].

Therefore, herein, we investigated ALD-Y_2O_3 thin films using Bis(methylcyclopentadienyl) (N'-isopropyl-N-n-propylacetamidinate)Yttrium ($Y(MeCp)_2$(iPr-nPrAMD)). ALD growth kinetics of $Y(MeCp)_2$(iPr-nPrAMD) were carefully examined. Also, the dependence of the growth rate and physical properties of Y_2O_3 thin films on the growth temperature was systematically analyzed. Finally, the etching resistance properties of ALD-Y_2O_3 thin films were thoroughly discussed in the context of fluorine-based plasma.

2. Materials and Methods

Y_2O_3 thin films were deposited on p-type Si (100) wafer by ALD at a growth temperature ranging from 150 to 290 °C. Bis(methylcyclopentadienyl)(N'-isopropyl-N-n-propylacetamidinate)Yttrium ($Y(MeCp)_2$(iPr-nPrAMD), iChems Co., Ltd., Hwaseong-si, Republic of Korea) precursor was used as the precursor for Y, and H_2O was used as a reactant. It is noted that $Y(MeCp)_2$(iPr-nPrAMD) and H_2O were kept in separate individual canisters and maintained at 120 °C and room temperature, respectively, to provide a sufficient vapor pressure. One ALD cycle of Y_2O_3 consisted of $Y(MeCp)_2$(iPr-nPrAMD) injection with 50 sccm Ar for 3 s, a purge injection with 50 sccm Ar for 20 s, an injection of H_2O reactant with 50 sccm for 2 s, and another 50 sccm Ar purge injection for 20 s. And, the chamber working pressure was maintained at 1.2×10^{-1} Torr. A set of ALD-Y_2O_3 thin films was deposited by changing the growth temperature from 150 to 290 °C. And, the Y_2O_3 thin films deposited at 150, 180, 220, 260, and 290 °C were designated as Y_2O_3-150, Y_2O_3-180, Y_2O_3-220, Y_2O_3-260, and Y_2O_3-290, respectively. The number of the repeated ALD cycles was intentionally controlled to have a similar film thickness of ~ 30 nm, regardless of the growth temperatures, in order to diminish the effect of the film thickness on the physical and chemical properties of Y_2O_3 thin films.

The film thickness as well as the corresponding refractive index was analyzed using spectroscopic ellipsometry (α-SE, J. A. Woollam Co., Inc., Lincoln, NE, USA). The crystal structure and thin film density were determined by X-ray diffraction (XRD) and X-ray reflectometry (XRR) using a Rigaku Smartlab diffractometer (D/MAX-2500V, Tokyo, Japan) with a Cu-$k_{\alpha 1}$ radiation. And, depth profile of the composition was studied by Auger electron spectroscopy (AES, PHI-710, ULVAC-PHI, Chigasaki, Japan). The surface was checked by atomic force microscopy (AFM). The high-density plasma resistance was studied using reactive ion etching (RIE, LABStar, TTL, Pyeongtaek, Gyeonggi-do, Korea) at a plasma power of 400 W and a pressure of 50 mTorr for 15 min, employing a mixed gas of Ar (50 sccm), CF_4 (45 sccm), and O_2 (5 sccm).

3. Results and Discussion

First, the self-limiting growth of the ALD-Y_2O_3 thin films was studied. Figure 1a shows the growth rate of Y_2O_3 thin films as a function of $Y(MeCp)_2$(iPr-nPrAMD) pulse time to confirm the ALD reaction mechanism at a constant growth temperature of 260 °C. Other pulses in one ALD cycle, except for the $Y(MeCp)_2$(iPr-nPrAMD) precursor pulse time, were fixed to a 20 s purge, H_2O reactant for 10 s, and another 20 s purge. By increasing the $Y(MeCp)_2$(iPr-nPrAMD) pulse time from 2 s to 5 s, the growth rate increased and then saturated to 0.11 nm/cycle above 3 s. And, this result indicates that $Y(MeCp)_2$(iPr-nPrAMD) was chemisorbed in a self-limiting manner. Figure 1b shows the growth rate of Y_2O_3 thin films depending on the H_2O pulse time at 260 °C. In this case, the pulses for $Y(MeCp)_2$(iPr-nPrAMD), precursor purge, and reactant purge were fixed at 3 s, 20 s, and 20 s, respectively. As shown in Figure 1b, the growth rate of Y_2O_3 thin films was saturated to ~0.11 nm/cycle above 2 s, confirming that 2 s of H_2O pulse was enough to completely react with chemisorbed $Y(MeCp)_2$(iPr-nPrAMD) precursor. Thus, the saturated growth rate of Y_2O_3 thin films was confirmed to be ~0.11 nm/cycle at 260 °C. Another important aspect of ALD is that the film thickness can be digitally controlled by the repeated ALD cycles. Therefore, we investigated the dependence of Y_2O_3 film thickness as a function of the repeated ALD cycles, as shown in Figure 1c. As shown in Figure 1c, the thicknesses of Y_2O_3 were increased linearly with increasing ALD-Y_2O_3 cycles from 300 to 900. Also, the extrapolated line shows a negligible growth delay, indicating a rapid nucleation of Y_2O_3 by ALD. Next, we investigated the effect of growth temperatures on the growth rate and refractive index of Y_2O_3 thin films as shown in Figure 1d. With increasing the growth

temperatures from 150 to 290 °C, the growth rate of Y_2O_3 exhibited a nearly constant growth rate and did not exhibit CVD growth, suggesting a wide ALD temperature window of Y_2O_3. Additionally, an almost similar refractive index of ~1.87, with consideration to that (1.9) of bulk Y_2O_3 [12], was obtained within the ALD temperature window. Since the refractive index of a film generally depends on the film density [32], it was expected that a similar film density can be obtained from 150 to 290 °C. Also, it needs to be mentioned that the self-decomposition temperature of $Y(MeCp)_2$(iPr-nPrAMD) precursor could be higher than 290 °C, potentially extending the upper limit of the ALD temperature window, although this could not be confirmed due to the temperature limitation of the ALD equipment used.

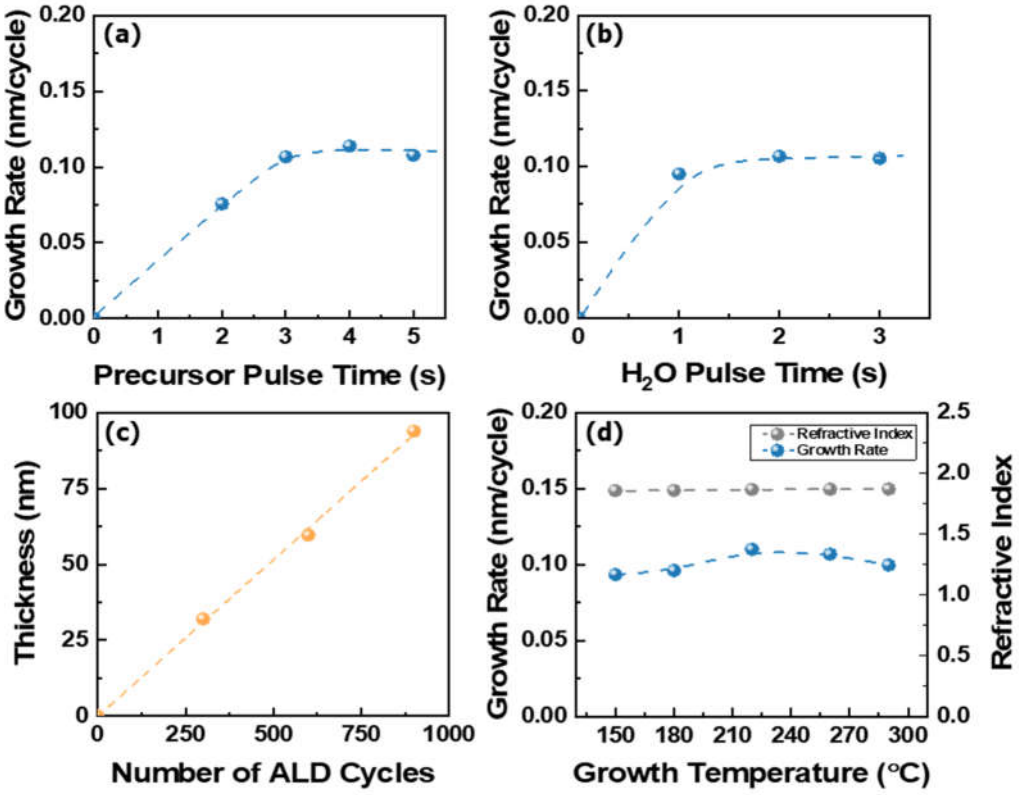

Figure 1. Growth rate of ALD-Y_2O_3 thin films depending on (**a**) the $Y(MeCp)_2$(iPr-nPrAMD) pulse time and (**b**) H_2O pulse time at a growth temperature of 260 °C. (**c**) thickness of ALD-Y_2O_3 thin films as a function of the number of ALD cycles at a growth temperature of 260 °C. And, (**d**) growth rate and refractive index of ALD-Y_2O_3 thin films depending on the growth temperature from 150 to 290 °C.

The microstructures of Y_2O_3 thin films depending on the growth temperature were investigated by XRD, as shown in Figure 2a. It is worth mentioning that XRD patterns were obtained from the Y_2O_3 thin films having similar thicknesses of ~30 nm by controlling ALD cycles considering the obtained growth rate at each temperature shown in Figure 1d. As shown in Figure 2a, all the Y_2O_3 thin films exhibited a typical cubic polycrystalline phase of Y_2O_3 (JCPDS 31-1105) with (222), (400), (431), and (440) planes, regardless of the growth temperatures. These characteristic phases were observed even at a low growth temperature of 150 °C, likely due to the highly dense and pure Y_2O_3 film formation. However, as the growth temperature increases, the amount of Y_2O_3 (222) planes becomes dominant due to the higher thermal energy, which is consistent with previous reports [24,30]. Therefore, the effect of growth temperature on the film density was investigated by XRR analysis, as shown in Figure 2b. The film densities were extracted from the location of the critical angles shown in Figure 2b. And, the film densities of Y_2O_3-150, Y_2O_3-180, Y_2O_3-220, Y_2O_3-260, and Y_2O_3-290 samples were revealed to be 4.88 g/cm^3, 4.95 g/cm^3, 5.0 g/cm^3, 4.94 g/cm^3,

and 4.98 g/cm^3, respectively. Regardless of the growth temperatures, the film densities of all the Y_2O_3 thin films were close to the bulk density (5.03 g/cm^3) of Y_2O_3, supporting the well-crystallized phases even for the films grown at 150 °C in the XRD observation. Similarly, it can explain the similar value (~1.87) of refractive indexes within the ALD temperature window.

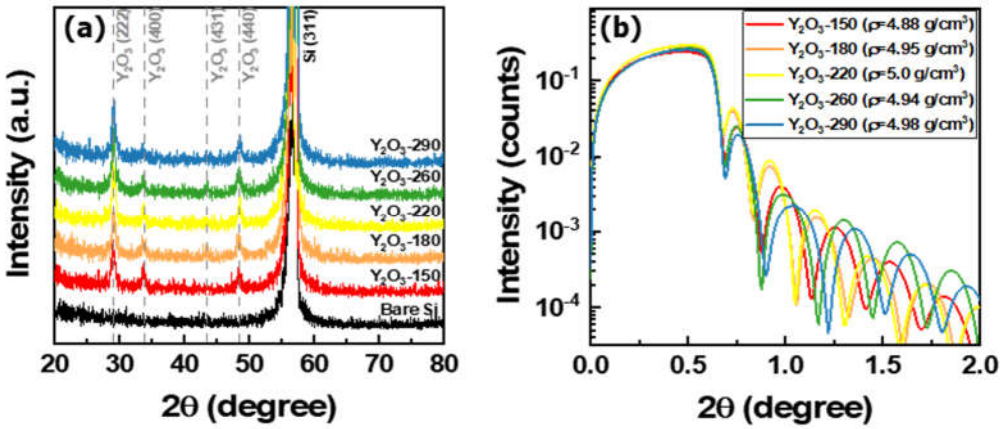

Figure 2. (**a**) XRD and (**b**) XRR patterns of ALD-Y_2O_3 thin films depending on the deposition temperatures from 150 to 290 °C.

An AES depth profile study was also performed to investigate the effect of growth temperature on the compositions and impurities of the Y_2O_3 thin films, as shown in Figure 3. For this, ALD-Y_2O_3 thin films grown at 150 and 290 °C were selected. As shown in Figure 3a,b, it showed that a stoichiometric Y_2O_3 thin film was successfully formed by ALD. Also, carbon impurities were below the detection limit of AES, which implies the ligands of $Y(MeCp)_2$(iPr-nPrAMD) precursor were completely removed even at a low temperature of 150 °C by an optimized ALD process. Thus, ALD-Y_2O_3 thin film resulted in high purity and high density, analogous to the Y_2O_3 bulk, and is a promising film for various applications including a protective coating against CF_4 based plasma.

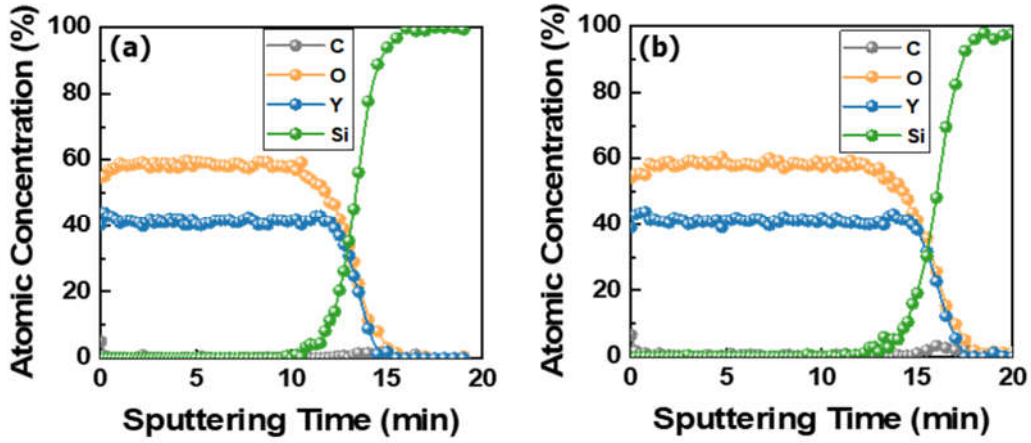

Figure 3. AES depth profiles of ALD-Y_2O_3 thin films prepared at a deposition temperature of (**a**) 150 °C and (**b**) 290 °C.

The plasma etching rate of ALD-Y_2O_3 thin films prepared at growth temperatures ranging from 150 to 290 °C was investigated using RIE at a plasma power of 400 W and a pressure of 50 mTorr, employing a mixed gas of Ar (50 sccm), CF_4 (45 sccm), and O_2 (5 sccm), as shown in Figure 4. Among the etching gases used, Ar induces only physical etching due to its chemical stability. CF_4 is generally known to influence both chemical and physical etching, while O_2 is employed to remove carbon from the film or Si by forming

CO_2 gas, as carbon is generated by the decomposition of CF_4. For the plasma etching process, ~30 nm thick-Y_2O_3 thin films were used. And, Al_2O_3 thin film with a thickness of ~110 nm was prepared at 150 °C by ALD in order to compare its etching behavior with that of ALD-Y_2O_3 thin films. After performing the RIE process for 15 min, the plasma etching rate was calculated based on the thickness difference of the films before and after RIE. As shown in Figure 4, Y_2O_3 thin films prepared at 150 °C exhibited a low plasma etching rate of 0.77 nm/min, while Al_2O_3 thin films prepared at the same temperature exhibited a very high plasma etching rate of 4.6 nm/min, which is approximately 6 times higher than that of the Y_2O_3 thin films.

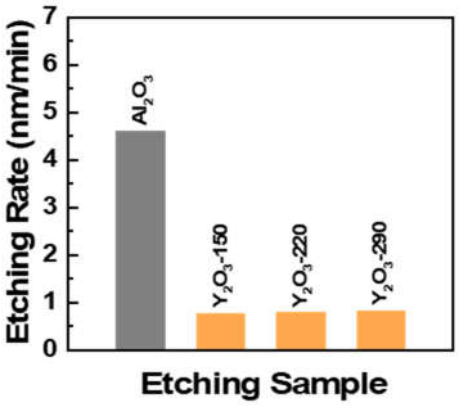

Figure 4. Plasma etching rate of ALD-Al_2O_3 and ALD-Y_2O_3 thin films, which was calculated based on the thickness difference of the films before and after RIE for 15 min.

The disparity in the plasma etching rate between the two materials indicates that the Y_2O_3 thin film exhibits greater resistance to $Ar/CF_4/O_2$ plasma compared to the Al_2O_3 thin film. Also, it is noteworthy that the growth temperature had minimal impact on the dry etching gas conditions for Y_2O_3 thin films. This is attributed to the high purity and high density of ALD-Y_2O_3 thin films using $Y(MeCp)_2$(iPr-nPrAMD) precursor and H_2O, regardless of the growth temperature.

These results can be explained by the fluorination plasma chemical etching reactions of Y_2O_3 and Al_2O_3 thin films:

$$Y_2O_3\ (s) + 3/2\ CF_4\ (g) \rightarrow 2\ YF_3\ (s) + 3/2\ CO_2\ (g) \quad (1)$$

$$Al_2O_3\ (s) + 3/2\ CF_4\ (g) \rightarrow 2\ AlF_3\ (s) + 3/2\ CO_2\ (g) \quad (2)$$

According to the fluorination reaction formulas described above, Y_2O_3 and Al_2O_3 thin films are generally fluorinated from the surface, forming YF_3 and AlF_3 surface layers, while CO_2 is removed by a vacuum system. During this process, YF_3 and AlF_3 surface layers are spontaneously formed due to the negative values of the standard enthalpy of formation and the standard Gibbs free energy of fluorination reactions [33]. In our case, therefore, similar YF_3 and AlF_3 thin films could be formed on Y_2O_3 and Al_2O_3 thin films, when Y_2O_3 and Al_2O_3 thin films were exposed to $Ar/CF_4/O_2$ plasma during the RIE. The formation of a YF_3 surface layer can reduce the erosion rate of Y_2O_3 thin films due to its high boiling temperature (2230 °C), while the AlF_3 surface layer can similarly reduce the erosion rate of Al_2O_3. However, the lower boiling temperature of AlF_3 (1291 °C) indicates that YF_3 is less prone to evaporation. Moreover, it was reported that the physical etching rate of AlF_3 is much faster than YF_3, while the physical etching rates are almost similar between Al_2O_3 and Y_2O_3 [34]. Therefore, the high difference in the plasma etching rate of Y_2O_3 and Al_2O_3 can be explained by a continuous surface fluorination reaction and its physical etching rates. Consequently, Y_2O_3 experiences less plasma erosion than Al_2O_3, suggesting that

ALD-Y_2O_3 using $Y(MeCp)_2$(iPr-nPrAMD) precursor and H_2O is a promising protective coating compared to ALD-Al_2O_3.

4. Conclusions

The ALD-Y_2O_3 process using the $Y(MeCp)_2$(iPr-nPrAMD) precursor and H_2O as the reactant demonstrated a wide ALD temperature window from 150 to 290 °C, with a consistent growth rate and refractive index. Additionally, ALD Y_2O_3 thin films exhibited a typical cubic polycrystalline phase, regardless of the growth temperature, primarily due to their high purity and density, similar to bulk Y_2O_3. The plasma etching rate of ALD-Y_2O_3 thin films grown at various temperatures was investigated using RIE at a plasma power of 400 W with a mixed gas of $Ar/CF_4/O_2$. For comparison, the plasma etching rate of ALD-Al_2O_3 thin films was also studied. When a growth temperature of 150 °C was applied to both ALD-Al_2O_3 and Y_2O_3 thin films, ALD-Y_2O_3 exhibited a significantly lower plasma etching rate compared to ALD-Al_2O_3. The difference in plasma etching rates between Y_2O_3 and Al_2O_3 was explained in detail based on continuous surface fluorination reactions and physical etching rates. Furthermore, it was observed that the growth temperature had minimal impact on the dry etching behavior of Y_2O_3 thin films. Based on these results, ALD-Y_2O_3 using the $Y(MeCp)_2$(iPr-nPrAMD) precursor and H_2O can be considered a promising protective coating for semiconductor components, outperforming Al_2O_3 in this regard.

Author Contributions: Conceptualization, H.K. and S.K.; methodology, S.K.; investigation, S.L.; data curation, S.L.; writing—original draft preparation, S.L.; writing—review and editing, S.K.; visualization, S.L.; supervision, S.K.; project administration, S.K.; funding acquisition, S.K. All authors have read and agreed to the published version of the manuscript.

Funding: This work was supported by the Korea Planning & Evaluation Institute of Industrial Technology (KEIT) grants funded by Ministry of Trade, Industry & Energy (MOTIE, Korea) (Technology Innovation Program, G01004064821 and K_G012001147505).

Institutional Review Board Statement: Not applicable.

Informed Consent Statement: Not applicable.

Data Availability Statement: Data are contained within the article.

Conflicts of Interest: Hyunchang Kim is employed by iChems Co., Ltd. The remaining authors declare that the research was conducted in the absence of any commercial or financial relationships that could be construed as a potential conflict of interest.

References

1. Kim, D.M.; Oh, Y.S.; Kim, S.W.; Kim, H.T.; Lim, D.S.; Lee, S.M. The erosion behaviors of Y_2O_3 and YF_3 coatings under fluorocarbon plasma. *Thin Solid Film.* **2011**, *519*, 6698–6702. [CrossRef]
2. Doemling, M.F.; Rueger, N.R.; Oehrlein, G.S.; Cook, J.M. Photoresist erosion studied in an inductively coupled plasma reactor employing CHF_3. *J. Vac. Sci. Technol. B* **1998**, *16*, 1998–2005. [CrossRef]
3. Cardinaud, C.; Peignon, M.C.; Tessier, P.Y. Plasma etching: Principles, mechanisms, application to micro-and nano-technologies. *Appl. Surf. Sci.* **2000**, *164*, 72–83. [CrossRef]
4. Ito, N.; Moriya, T.; Uesugi, F.; Matsumoto, M.; Liu, S.; Kitayama, Y. Reduction of Particle Contamination in Plasma-Etching Equipment by Dehydration of Chamber Wall. *Jpn. J. Appl. Phys.* **2008**, *47*, 3630–3634. [CrossRef]
5. Cunge, G.; Inglebert, R.L.; Joubert, O.; Vallier, L.; Sadeghi, N. Ion flux composition in $HBr/Cl_2/O_2$ and $HBr/Cl_2/O_2/CF_4$ chemistries during silicon etching in industrial high-density plasmas. *J. Vac. Sci. Technol. B* **2002**, *20*, 2137–2148. [CrossRef]
6. Fukumoto, H.; Fujikake, I.; Takao, Y.; Eriguchi, K.; Ono, K. Plasma chemical behaviour of reactants and reaction products during inductively coupled CF_4 plasma etching of SiO_2. *Plasma Sources Sci. Technol.* **2009**, *18*, 045027. [CrossRef]

7. Miwa, K.; Sawai, T.; Aoyama, M.; Inoue, F.; Oikawa, A.; Imaoka, K. Particle reduction using Y_2O_3 material in an etching tool. In Proceedings of the 2007 International Symposium on Semiconductor Manufacturing, Santa Clara, CA, USA, 15–17 October 2007; pp. 1–4.
8. Iwasawa, J.; Nishimizu, R.; Tokita, M.; Kiyohara, M.; Uematsu, K. Plasma-Resistant Dense Yttrium Oxide Film Prepared by Aerosol Deposition Process. *J. Am. Ceram. Soc.* **2007**, *90*, 2327–2332. [CrossRef]
9. Qin, X.; Zhou, G.; Yang, H.; Wong, J.I.; Zhang, J.; Luo, D.; Wang, S.; Ma, J.; Tang, D. Fabrication and plasma resistance properties of transparent YAG ceramics. *Ceram. Int.* **2012**, *38*, 2529–2535. [CrossRef]
10. Kim, D.M.; Lee, S.H.; Alexander, W.B.; Kim, K.B.; Oh, Y.S.; Lee, S.M. X-Ray Photoelectron Spectroscopy Study on the Interaction of Yttrium–Aluminum Oxide with Fluorine-Based Plasma. *J. Am. Ceram. Soc.* **2011**, *94*, 3455–3459. [CrossRef]
11. Alarcón-Flores, G.; Aguilar-Frutis, M.; Falcony, C.; García-Hipolito, M.; Araiza-Ibarra, J.J.; Herrera-Suárez, H.J. Low interface states and high dielectric constant films on Si substrates. *J. Vac. Sci. Technol. B.* **2006**, *24*, 1873. [CrossRef]
12. Rouffignac, P.; Park, J.S.; Gordon, R.G. Atomic layer deposition of Y_2O_3 Thin Films from Yttrium Tris(N,N′-diisopropylacetamidinate) and Water. *Chem. Mater.* **2005**, *17*, 4808. [CrossRef]
13. Klein, P.H.; Croft, W.J. Thermal Conductivity, Diffusivity, and Expansion of Y_2O_3, $Y_3Al_5O_{12}$, and LaF_3 in the Range 77°–300°K. *J. Appl. Phys.* **1967**, *38*, 1603–1607. [CrossRef]
14. Fan, W.; Bai, Y.; Wang, Z.Z.; Che, J.W.; Wang, Y.; Tao, W.Z.; Wang, R.J.; Liang, G.Y. Effect of point defects on the thermal conductivity of Sc_2O_3-Y_2O_3 co-stabilized tetragonal ZrO_2 ceramic materials. *J. Eur. Ceram. Soc.* **2019**, *39*, 2389–2396. [CrossRef]
15. Wilk, G.D.; Wallace, R.M.; Anthony, J.M. High-κ gate dielectrics: Current status and materials properties considerations. *J. Appl. Phys.* **2001**, *89*, 5243–5275. [CrossRef]
16. Kim, M.; Choi, E.; Lee, D.; Seo, J.; Back, T.S.; So, J.; Yun, J.Y.; Suh, S.M. The effect of powder particle size on the corrosion behavior of atmospheric plasma spray-Y_2O_3 coating: Unraveling the corrosion mechanism by fluorine-based plasma. *Appl. Surf. Sci.* **2022**, *606*, 154958. [CrossRef]
17. Kitamura, J.; Ibe, H.; Yuasa, F.; Mizuno, H. Plasma sprayed coatings of high-purity ceramics for semiconductor and flat-panel-display production equipment. *J. Therm. Spray Technol.* **2008**, *17*, 878–886. [CrossRef]
18. Wiktorczyk, T.; Biegański, P.; Serafińczuk, J. Optical properties of nanocrystalline Y_2O_3 thin films grown on quartz substrates by electron beam deposition. *Opt. Mater.* **2016**, *59*, 150–156. [CrossRef]
19. Varhue, W.J.; Massimo, M.; Carrulli, J.M.; Baranauskas, V.; Adams, E.; Broitman, E. Deposition of Y_2O_3 by plasma enhanced organometallic chemical vapor deposition using an electron cyclotron resonance source. *J. Vac. Sci. Technol. A* **1993**, *11*, 1870–1874. [CrossRef]
20. Detavernier, C.; Dendooven, J.; Sree, S.P.; Ludwig, K.F.; Martens, J.A. Tailoring nanoporous materials by atomic layer deposition. *Chem. Soc. Rev.* **2011**, *40*, 5242. [CrossRef]
21. Cremers, V.; Puurunen, R.L.; Dendooven, J. Conformality in atomic layer deposition: Current status overview of analysis and modelling. *Appl. Phys. Rev.* **2019**, *6*, 021302. [CrossRef]
22. Johnson, R.W.; Hultqvist, A.; Bent, S.F. A brief review of atomic layer deposition: From fundamentals to applications. *Mater. Today* **2014**, *17*, 236. [CrossRef]
23. Muñoz-Rojasu, D.; Maindron, T.; Esteve, A.; Piallat, F.; Kools, J.C.S.; Decams, J.M. Speeding up the unique assets of atomic layer deposition. *Mater. Today Chem.* **2019**, *12*, 96. [CrossRef]
24. Niinistö, J.; Putkonen, M.; Niinistö, L. Processing of Y_2O_3 Thin Films by Atomic Layer Deposition from Cyclopentadienyl-Type Compounds and Water as Precursors. *Chem. Mater.* **2004**, *16*, 2953. [CrossRef]
25. Majumder, P.; Jursich, G.; Kueltzo, A.; Takoudis, C. Atomic Layer Deposition of Y_2O_3 Films on Silicon Using Tris(ethylcyclopentadienyl) Yttrium Precursor and Water Vapor. *J. Electrochem. Soc.* **2008**, *155*, G152. [CrossRef]
26. Xu, R.; Selvaraj, S.K.; Azimi, N.; Takoudis, C.G. Growth Characteristics and Properties of Yttrium Oxide Thin Films by Atomic Layer Deposition from Novel $Y(iPrCp)_3$ Precursor and O_3. *ECS Trans.* **2012**, *50*, 107. [CrossRef]
27. Gusev, E.P.; Cartier, E.; Buchanan, D.A.; Gribelyuk, M.; Copel, M.; Okorn-Schmidt, H.; D'Emic, C. Ultrathin high-K metal oxides on silicon: Processing, characterization and integration issues. *Microelectron. Eng.* **2001**, *59*, 341. [CrossRef]
28. Van, T.T.; Chang, J.P. Radical-enhanced atomic layer deposition of Y_2O_3 via a β-diketonate precursor and O radicals. *Surf. Sci.* **2005**, *596*, 1–11. [CrossRef]
29. Mölsä, H.; Niinistö, L.; Utriainen, M. Growth of yttrium oxide thin films from β-diketonate precursor. *Adv. Mater. Opt. Electron.* **1994**, *4*, 389. [CrossRef]
30. Putkonen, M.; Sajavaara, T.; Johansson, L.S.; Niinistö, L. Low-Temperature ALE Deposition of Y_2O_3 Thin Films from β-Diketonate Precursors. *Chem. Vap. Depos.* **2001**, *7*, 44. [CrossRef]
31. Dussarrat, C.; Blasco, N.; Noh, W.; Lee, J.; Greet, J.; Teramoto, T.; Kamimura, S.; Gosset, N.; Ono, T. Thermal Atomic Layer Deposition of Yttrium Oxide Films and Their Properties in Anticorrosion and Water Repellent Coating Applications. *Coatings* **2021**, *11*, 497. [CrossRef]

32. Mergel, D.; Buschendort, D.; Eggert, S.; Grammes, R.; Samset, B. Density and refractive index of TiO_2 films prepared by reactive evaporation. *Thin Solid Films* **2000**, *371*, 218. [CrossRef]
33. Cao, Y.C.; Zhao, L.; Luo, J.; Wang, K.; Zhang, B.P.; Yokota, H.; Ito, Y.; Li, J.F. Plasma etching behavior of Y_2O_3 ceramics: Comparative study with Al_2O_3. *Appl. Surf. Sci.* **2016**, *366*, 304. [CrossRef]
34. Kim, D.M.; Jang, M.R.; Oh, Y.S.; Kim, S.K.; Lee, S.M.; Lee, S.H. Relative sputtering rates of oxides and fluorides of aluminum and yttrium. *Surf. Coat. Technol.* **2017**, *309*, 694. [CrossRef]